Muath S. Talafha
Ph.D. student
Hungarian University of agriculture and life science
mechanical engineering doctoral school
Hungary

István Oldal
Professor
Hungarian University of agriculture and life science
mechanical engineering doctoral school
Hungary

Seifeddine Garneoui
Ph.D. student
Hungarian University of agriculture and life science
mechanical engineering doctoral school
Hungary

Study the Particle Size Impact on the Mechanical Behaviour of Granular Material by Discrete Element Method

Granular materials are used in various industries, including pharmaceutical and agriculture, where the material properties of elements have an important impact on their flow behavior. Numerical codes based on the Discrete Element Method (DEM) are decisive for describing the flow of granular material. The DEM could investigate granular materials' macro and micro-mechanical shear behaviors. The commercial software EDEM® based on the DEM was utilized for this purpose. A gravitational disposition for the geometrical arrangement model has been performed in this study to model different particle sizes for a direct, simple shear test (DSST). The results indicated that referring to the size index (SI), a positive correlation occurred with the shear strength, dilation, volumetric strain, a negative correlation with the average particle angular velocity, and a neutral correlation with the coordination number (CN).

Keywords: *Discrete element method; Granular material; Particle shape; Simple direct shear test; Size index.*

1. INTRODUCTION

Granular material is the primary component in the pharmaceutical and agricultural industries[1]. There are a lot of factors that affect the mechanical behavior of the granular material bed, such as loading properties [2], fouling level [3], distribution of particle size [4], the void ratio [5], normal stress and confining pressure [6]; In addition to the individual particle properties: particle size[7], particle shape [8], and strength[9] have an impact on the mechanical behavior. The key para–meters determining the response of granular materials are the angularity and surface texture of the particles [10]. It has been revealed that particle degradation depends on particle shape[11]. Complex-shaped partic–les are more likely to break than cubic particles; how–ever, in the experimental study, it is challenging to provide a straightforward approach to find the evolu–tion of particle angularity/texture during the shear test due to the costly experiments and the large-scale limi–tation. Therefore DEM simulations are applied instead to investigate the behavior of granular materials.

Because of the drawbacks mentioned above, DEM models have been developed to study the behavior of granular materials for decades. Moreover, DEM allows analyzing the results achieved by varying the parameters of the simulated materials, particularly the shape index [12]. It was demonstrated in a previous study where authors used two-dimensional simulations that revealed the shear strength, dilatation, and latent shear strength increased as the particles' angularity raised [13]. On the other hand, describing such par–ticles' actual shape in DEM simulations is still challenging. At the beginning of DEM simulations, the description of a real particle shape could only be modeled using a disk or a sphere [14]. Despite the simple DEM algorithm for detecting the interactions and measuring forces, the actual structure of a particle needs to be modeled because using a regular shape such as a disk or sphere would provide appropriate rolling resistance compared to the original particle shape. When considering particles as disks or spheres, their rotation is solely influenced by the tangential component of the contact force; the moment on such particles has no effect since the normal force is oriented towards the center [15-17]. These techni–ues have been used in railway research to model ballast particle shapes.

In a previous study, the behavior of a ballast settlement was analyzed through DEM using polygon-shaped elements to mimic the actual shape of the ballast particulates under dynamic loading [18]. Researchers revealed that particles having a size inferior to half of the nominal maximum size of the actual particle are inadequate to conduct a full-scale ballast layers simulation [19]. In another work, a similar approach was utilized when modeling ballast layers [20,21], while another study produced a 2D projection of complex-shaped ballast particles using clusters of bonded circular particles [22].In conclusion, 3D simulations have been conducted to model ballast similarly [23]. However, ellipsoidal particles [15], elliptical particles with oval-shaped boundaries [24], particles shaped like polygons [25], particles with dense clusters overlapping [16], and particles with axial symmetry may not adequately describe the actual shapes of these particles [26].

Furthermore, a few of these methods need signi–ficant computing time. Therefore, to simulate the particle form, researchers presented an approach based on a simple algorithm widely used in DEM; in this procedure, the overlapping spherical components are

Received: March 2020, Accepted: July 2020
Correspondence to: Muath S. Talafha, Hungarian University of agriculture and life science, Gödöllö, H-2103, Hungary.
E-mail: muath.talafha@gmail.com
doi:10.5937/fme2203473T

tightly joined, which offers the advantage of modeling a particle shape with varying angularities while fol–lowing the same contact laws as a single sphere [27]. Modeling the real shape of ballasts has been done using this method. Researchers simulated The geogrid-reinforced ballasts to decide the ideal position for a geogrid [28].

While most numerical studies tackled the modeling of actual particle shapes and the mechanical responses of the ballast layer under different situations, the effects of the particle shape on the mechanical results, which are complex to analyze in laboratory experiments, are cumbersome in the literature. Moreover, due to the minimal friction between particles, scientists conducted a simple direct shear test, proving that when using a fouled particle, the particle's shear strength decreased due to a reduction in the friction angle[29]. They Moreover found that dilation occurs in the fouled ballast sample by applying a high rate of fouled particles, particularly at a low normal stress level. Additionally, employing a geogrid was in prime agreement with DEM simulation and lab data of coal-fouled ballasts [30].In conclusion, the sleepers' side resistance was reduced using fouling particles in the ballast bed, especially when fouling particles were placed at the edge of the ballast bed [31].

Researchers have studied the random shape and size of the particles in terms of angularity index AI where the AI analyzes the particle in terms of the number and sharpness of the corners [32], and the sphericity index SPH which the SPHrepresents how closely an object's shape matches a whole complete sphere [33]. Therefore, a new study path has been established by studying particles with a definite shape and size. For instance, this new study path has exa–mined the effect of different SPH for the same definite particle size [34] and different size index SI for a certain shape triple particle, where the SI represents the size variations of a definite particle shape [35]. In addition, the main objective of this study is to examine the effect of double particle size index SI on the particles' mechanical behavior in the direct, simple shear test (DSST).

2. THE DISCRETE ELEMENT METHOD (DEM)

Instead of the conventional cost-effective trial-and-error method, the DEM is an excellent tool for modeling the mechanical properties of bulk material and a whole process of particle blending [36].

The Method of Discrete Elements (DEM) was deve–loped to simulate the mechanical behavior of granular materials. Newton's second law of motion describes the translational and rotational motion of every particle in the DEM system [37,38]. During the simulation circle, The normal and tangential forces generated among particles and between particles and the wall are computed using a calculation loop that involves apply–ing Newtonian equations of motion repeatedly to generate each particle's acceleration, velocity, and disp–lacement values, as described by the following equa–tions [36]:

$$F_t = -8G_0\sqrt{R_0\delta\delta_t} - 2\sqrt{\frac{5}{6}}\frac{\ln C_r}{\sqrt{\ln^2 C_r + \pi^2}}\sqrt{2G_0}\sqrt[4]{R_0\delta}\sqrt{m_0 v_{nrel}} \quad (1)$$

The young E_0 module equivalent of two inter–mingling particles is derived from the following formula.

$1/E_0 = \left(1-v_1^2\right)/E_1 + \left(1-v_2^2\right)/E_2 \cdot \delta$ Represents the amount when those two particles collide, and C_r is the coefficient of restitution (described in EDEM® [39] as the ratio of separation to approach speed in a collision). The normal overlap δ characterizes normal particle deformation.

$$F_t = -8G_0\sqrt{R_0\delta\delta_t} - 2\sqrt{\frac{5}{6}}\frac{\ln C_r}{\sqrt{\ln^2 C_r + \pi^2}}\sqrt{2G_0}\sqrt[4]{R_0\delta}\sqrt{m_0 v_{nrel}} \quad (2)$$

The equivalent shear modulus of two entangled particles G_0 is calculated using the following formula: $1/E_0 = \left(1-v_1^2\right)/E_1 + \left(1-v_2^2\right)/E_2 \cdot \delta$ Describes the tan gential overlap of two particles, representing the tan–gential deformation. Tangent overlap is the tangential movement between two particles from first to last contact, whether when one particle rolls or slips against another. And vtrel Is the tangential component of relative particle velocity.

The particles' recent displacement obtained is utilized to further calculate the contact forces and torques in that area of contact due to the particles' interactions in the newfound position. This simulation cycle is applied repeatedly through time to describe the flow of the bulk material [40]. This method is ideal for analyzing the movement of a granular material [41]and examining the vibration effect [40]. Researchers predicted that the DEM models might be used to deter–mine and analyze the pressure distribution in a silo by simplifying the design process for this sort of equipment [42]. DEM Furthermoreinvestigatesthe flow patterns, segregation, discharge rates, and the effect of flow patterns in silos [40]. The discrete element technique is powerful for illustrating particle motion in various scenarios. Torques are calculated using DEM based on particle displacement in every timestep. The behavior of particles and interactions highly depends on the particles' shape and the different micro-mechanical properties [40]. The commercial software EDEM® was used by adopting the"Hertz Mindlin No-Slip" contact model [39].

3. DEM SIMULATION OF THE SHEAR CYLINDER

The numerical experiments were carried out in a cylinder having a 225 mm height and a 52 mm radius, as illustrated in Figure 1. The lower part of the cylinder has a height of 75 mm and was set to move only horizontally, while the upper part of the150 mm height is fixed in all directions. The horizontal displacement of the lower part in the DEM model was allowed to move for a distance of 30mm (around 15% of shear strain), which is sufficient to reach the peak of particles' shear stress. The vertical loading test applied a constant normal load on the sample. The horizontal loading test applies a shear force to the sample at a constant displacement rate.

A definite number of particles having similar shapes and sizes were generated in each simulation. Then, the particles were packed into the cylindrical container under the effect of gravity and were allowed to repose until the bed's free-motion state reached. This initial state was considered for all the simulation cases. The simulation scenarios were executed in three stages. Initially, particles were rapidly generated through a factory into the cylinder where the kinetic energy dominates, and a high contact between particles occurred. Afterward, the generated particles require settling time, and null kinetic energy is attained. During the second stage, the material bed was subject to a vertical load by letting a ball with almost the same diameter as the cylinder fall on the particle bed; the ball's adjustable density allows to apply several vertical loads from the top of the DEM system. Furthermore, the spherical shape of the loading tool (ball) helps us avoid the particle bed's locking volume problem during the shear test as it lets the material bed freely move vertically even under loading, which is a common problem during DEM shear tests[43].

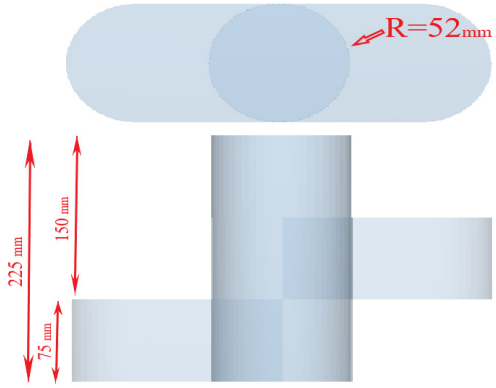

Figure 1 Schematic of model geometry

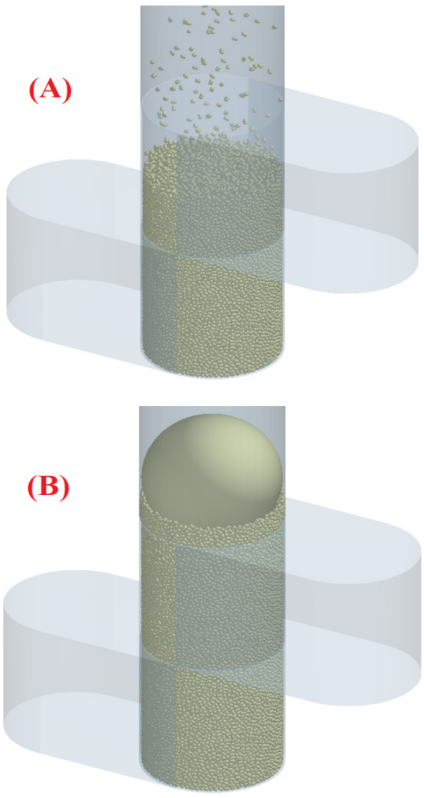

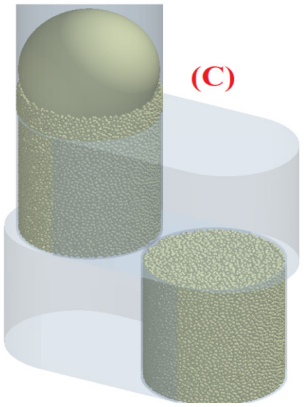

Figure 2 Shear box Simulation and assembled generation Stages particles with a 100% size ratio under 3 kPa normal pressure. (Articles generation, Bcompressedby normal stress, C shearing process)

The final step was accomplished by performing a direct, simple shear test by moving the lower cylinder of the model horizontally while maintaining the vertical load constant during the shear, as illustrated in figure 2.

3.1 Model Parameters

We simulated a large-scale model of the real direct, simple shear test cylinder using a solid wall and a deadweight sphere (ball) above the particles bed in the upper cylinder. This rearrangement allows the particle's volume to fluctuate freely during the shearing process. Figure 3 illustrates a defined SI for a five-particle used during the simulation. (Size Indexes= 50%, 75%, 100%, 125%, 150% for all the particles, respectively).During all the simulations, the particle size for each simulation was the same to minimize the degradation effect. The particle radius and the distance between the centers of the particles vary with each repetition: (R= 0.5mm, 0.75mm, 1mm, 1.25mm, and 1.5mm) as revealed in Fig 3. for each simulation scenario, particles with a particular shape and size were generated. The SI=50% assemblies have 596000 particles, SI=75% assemblies have 280000 particles, SI=100% assemblies have 110000 particles, SI=125% assemblies have 60000 particles, and SI=150% assemblies have 32000 particles. For each run, the normal gravity forces compact the identical SI particles that fill the shear cylinder, which is repeated for each simulation to allow a successful sample comparison.

Table 1. The model Micromechanical parameters.

Parameter	Value
Particles Poisson's ratio	0.4
Wall Poisson's ratio	0.3
Particles Shear modulus (Pa)	3.58×10^8
Wall Shear modulus (Pa)	8×10^8
Coefficient of restitution	0.5
Coefficient of rolling friction	0.01
Particle density (kg/m3)	1430
Coefficient of interparticle friction	0.5
Coefficient of plane wall-particle friction	0.6

Furthermore, the ratio distance between the clump centers was kept constant (sphericity index=88%) to preserve the same particle shape. Additionally, four different vertical loads were examined for each SI, and

since we have five different SI, the total number of simulations is twenty.

The DEM parameters in Table 1, based on the previous work, were used in our work to achieve accurate results [36,44].

3.2 Particle Shape Generation

A specific SI was considered for each simulation, with a constant SPH to analyze the effect of the SI on the particle's mechanical behavior.

Fig.3 illustrates all particles' SI values used in this study.

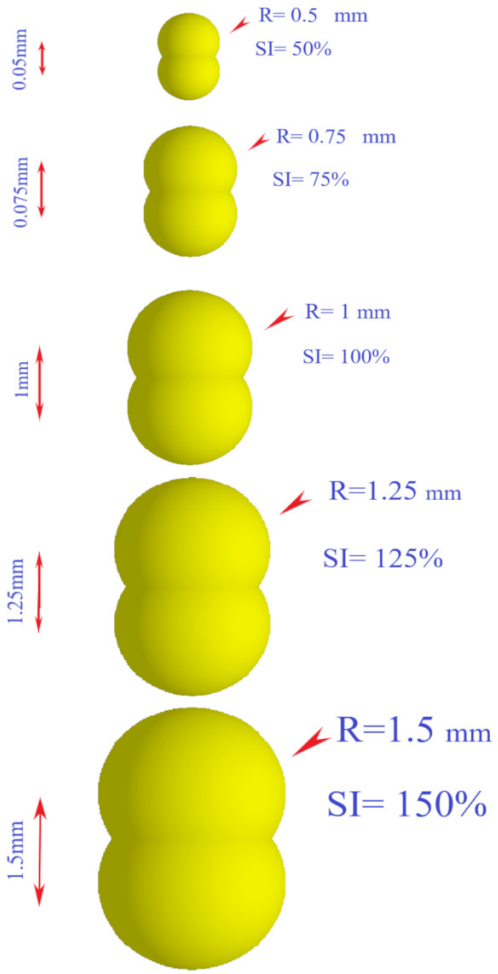

Figure 3. Various particle SI simulations(SI= 50%, 75%, 100%, 125%, 150% for all the particles respectively).

4. RESULTS AND DISCUSSION

This part summarises the particles bed macroscopic and microscopic findings of shear stress, network contact forces, variation of contact number, and average particle rotation in the DSST.

Shear Stress

The forthcoming graphs demonstrate the effect of SI on the relationship between the horizontal strain and the shear stress at a steady rate of normal stress. Furthermore, to calculate the internal friction angle, we measured the arctangent of the shear stress ratio with the normal stress ratio ($\varphi = \arctan(\tau.\sigma)$). Therefore, a positive correlation between the internal friction angle and the particle size is observed with an increase in particle size. The internal friction angle increases with particle size (SI). On the other hand, increasing the SI significantly influenced the findings; two-dimensional elliptical particles had similar outcomes [15]; in addition, 3D ellipsoid multi-sphere assemblies obtained a similar conclusion [45].

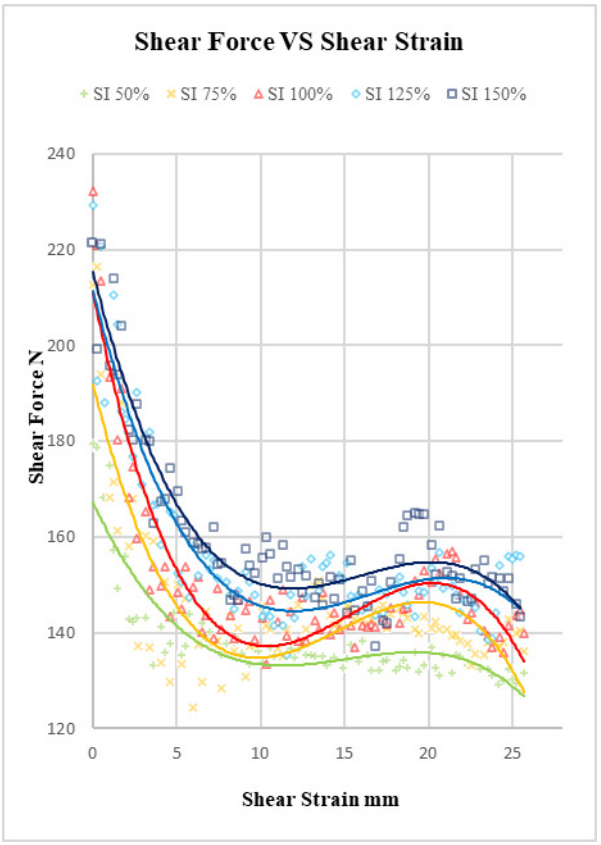

Figure 4 Shear force vs. shear displacement plots of samples with varying SI at 30kPa normal stress

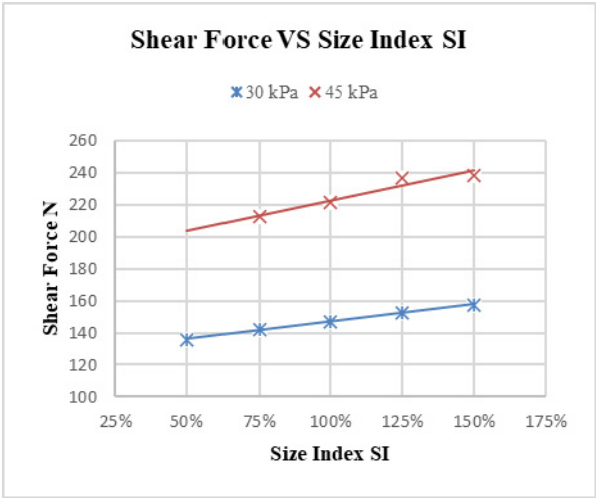

Figure 5 Shear stress with a variety of SI at 30 kPa and 45 kPa normal stress

Comparing particle samples, the influence of the SI is more apparent. This phenomenon illustrates the prog–ression of the moment force and the course interlocking connections between particles under normal stress

(course interaction between the particles). Due to the critical moment required for rotating particles, the large particles would be more frictionally interlocked. For example, at a30 kPa normal stress, the shear force increased from 136N to 158N when the particle SI changed from 50% to 150%. However, the change in shear force was decreased for smaller SI particles and vice versa.

Fig. 4is plotted to understand better the effects of the SI on the particles' shear behavior under constant normal stress.

Fig.5 illustrates that the interlocking particles can be dilated as the normal stress decreases, decreasing the total shear force. When the rate increases, the particle encounters a more effective interlocking rate, gradually increasing the shear stress. In contrast, due to the high normal stress, these particles would not move easily against each other, leading to anisotropy; therefore, the Friction angle is reduced in a sample with less aniso–tropy [46].

A rise in the shear stress occurs simultaneously with an increase in the SI. For example, in the case of 30 kPa normal stress, when the particles' SI increases from 50% to 150%, the sheer force increases by around 15%.

Volumetric Strain

Fig. 6 illustrates the volumetric strain variation with a horizontal strain under different normal stresses. A reverse correlation occurs between the overall volumetric strain and the normal stress; as the normal stress increases, the overall volumetric strain decrease and vice-versa. From this relationship, a lower dilation of particle volume strain occurs under a higher value of normal stress.

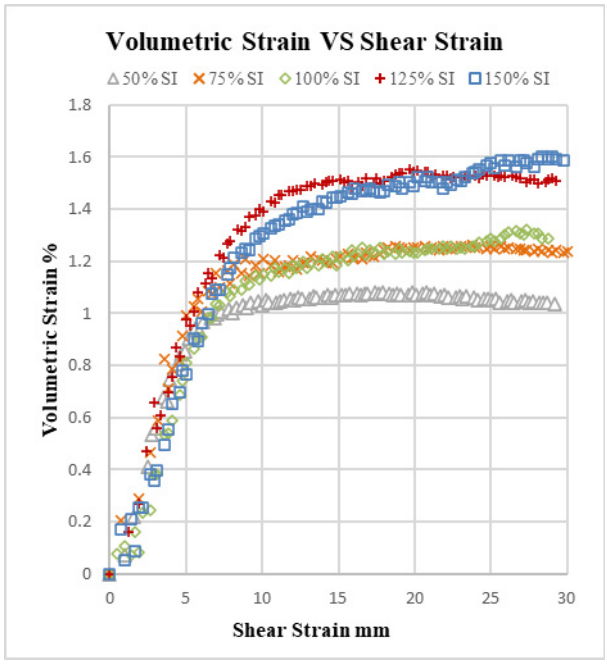

Figure 6 Variations of volumetric strain with shear strain for various normal stresses (SI 150%) Normal stress 30kPa, 45kPa, 60kPa

Fig. 7 illustrates that as the particle's SI increases, the particle volume dilation increase; therefore, it is clear that the particles' volume dilation depends on the particles' shape and the normal stress[34].

Fig.8 illustratesthat a lower level of dilation occurs at higher normal stresses. For example, in the case of a 30 kPa normal stress, The dilation value increase by 28% when the assembly particles' SI change from 50% to 150%.

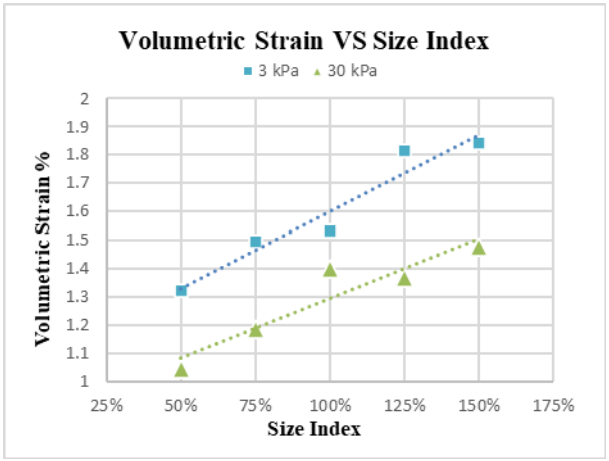

Figure 7 Variations of volumetric strain with shear strain for different size indexes at normal pressure of 30 kPa

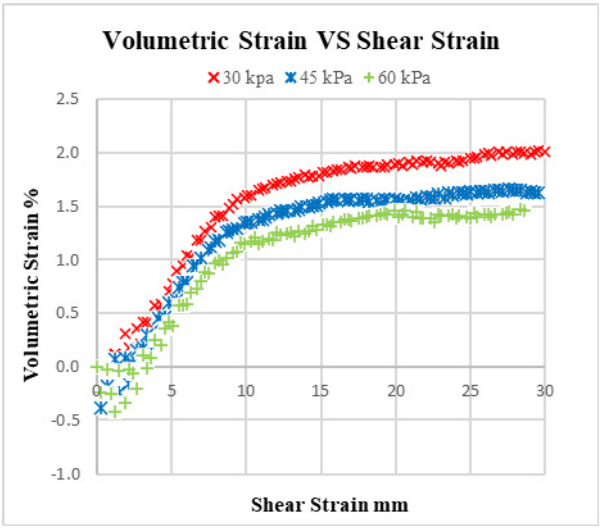

Figure 8 Volumetric strain for different size index values at a normal stress of 3 and 30kPa

4.3 Average Contact Numbers

Particle-to-particle contact ratio, or the coordination number (CN), where CN is the number of particles in contact with the total number of particles in the assembly, CN is a suitable parameter for describing granular materials' behavior since the particle interaction is related to points of contact[32].

As demonstrated in Fig.9, The CN is constant as the SI increases or decreases; the CN remains relatively constant when the SI changes. Therefore, it can be clarified that by increasing or decreasing the SI, the changes in particle shape happen in three dimensions, which means the particle size will change, but the particle shape will be preserved. Therefore, the density of the particle connections in the assembly will stay relatively constant since the SI change does not interfere with the sphericity of the particle. Thus, the sphericity

index will remain constant. Furthermore, researchers mentioned that in the case of changing the particle SPH, the particle shape changes in one dimension, making the particle more elongated, leading to increases in the interlocking between the particles; by giving other particles the chance to have contact with the same particle. In summary, increasing the CN[34].

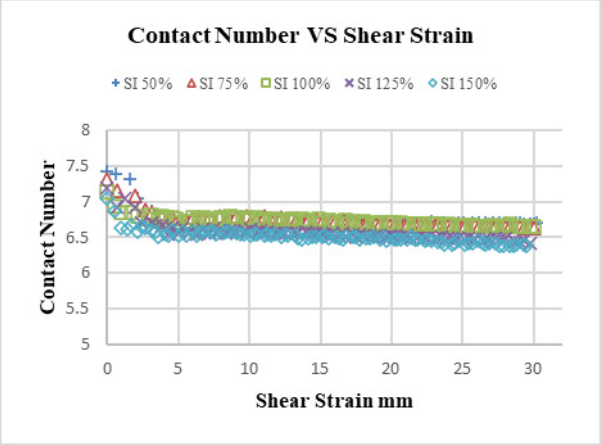

Figure 9 Variations of CN versus shear strain for normal stress of 30kPa (SI effect)

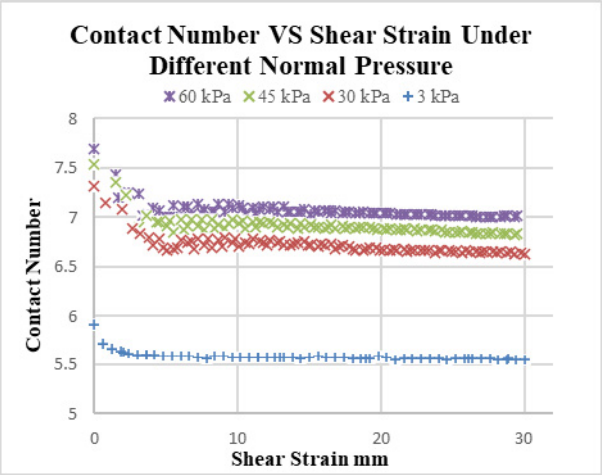

Figure 10 Variations of CN versus shear strain for various normal stresses (SI 150%)

Fig.10 illustratesthat a more significant CN was produced, independently of the SI index, when high pressure was applied to the sample. However, A drop in CN is immediately seen in lower normal stress levels due to dilatation caused by the first strain.

The Chain of Contact Force

Figures 11&12 illustrate the forces distribution in the model at different steps of the DSST, where the inter-particle and particle-wall forces are examined at different SI values and normal stresses. These figures also demonstrate the number of contact forces in the model, where the higher contact forces are represented in red, the moderate forces in green, and the low forces in blue. Before the first step by moving the lower cylinder and applying the shear stress (strain 0%), the particles in the model revealed a uniform distribution for all of the models with different particles' SI. However, contact force chain variations are noticeably different at a 15% strain than at a 0% strain when applied shear force. Fig.11 illustrates a thicker contact forces chain in the first stage of the simulation (0% strain) compared to Fig. 12, which demonstrates the simulation's second step (15% strain). The thicker contact forces are observed because of the dilation behavior of the particles during the shear, causing a decrease in the CN of the particles.

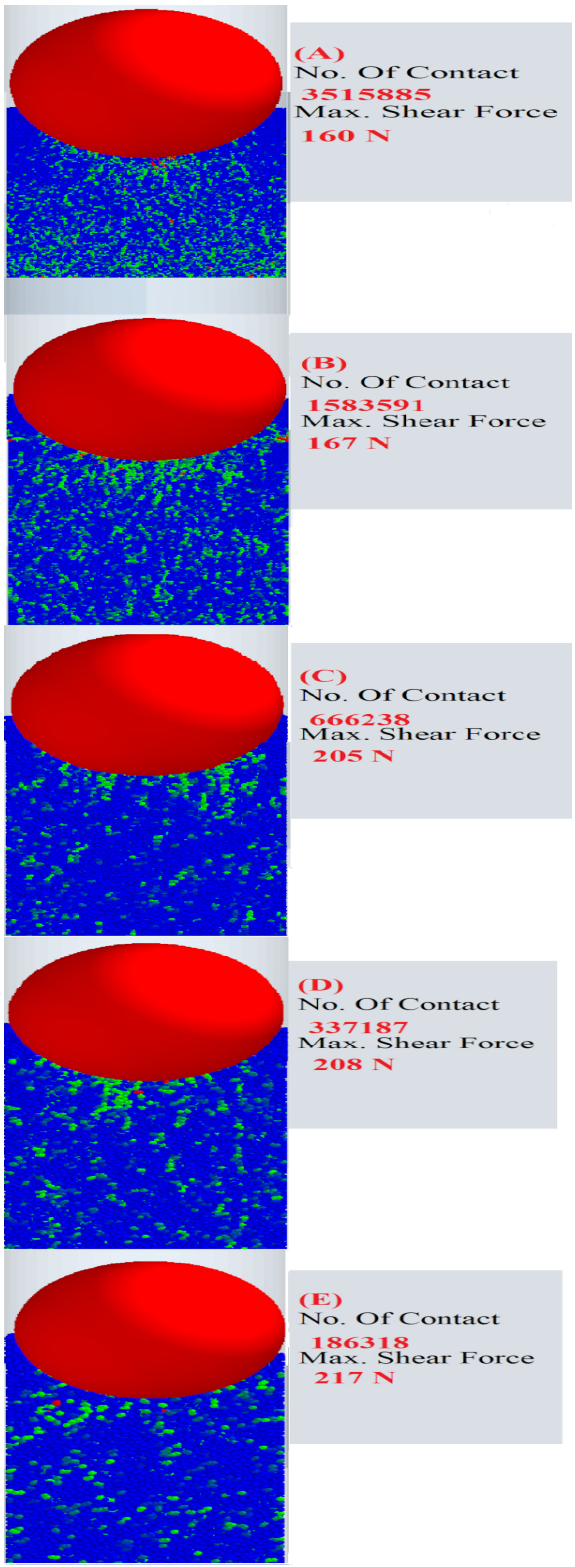

Figure 11 Distribution of contact force chains for various SI particles at shear strain of 0% and 30kPa normal stress (Size index SI= 50%, 75%, 100%, 125%, 150% respectively)

It can be observed from the shear stage that the particles' CN follow the direction of the higher loads (i.e., shear direction). As the shearing is applied to the model by moving the lower cylinder, it causes a reduction in the interaction cross-section area between the two cylinders, resulting in a gradual decrease in the shear stress.

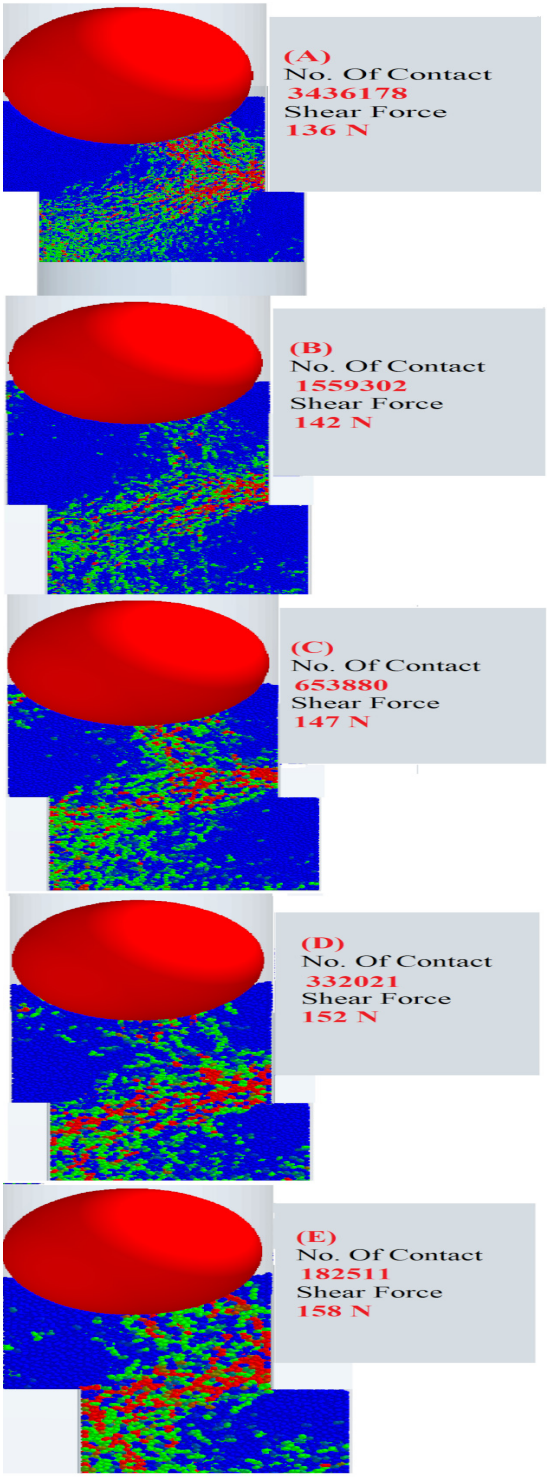

Figure 12 Distribution of contact force chains for various SIparticles at shear strain of 15% and 30kPa normal stress (Size index SI= 50%, 75%, 100%, 125%, 150% respectively)

Furthermore, the sample with a high SI value increases the shear force during the shear stage because of the higher coarse interaction (i.e., better interlocking) as the particles' SI increases. In addition, a study has similar results, which addressed higher force chains that shaped a greater particle contact in higher SI samples [47]. These circumstances of the mobile part, where the lower cylinder start to move in the right direction to apply the shearing stress, causes the shear band to form from the bottom left of the lower cylinder to the top right of the upper cylinder and hold the most of the load transmission in the assembly. As a result, a stable force chain structure formed. Simultaneously, any particle outside of the shearing band is not participating in carrying the load, as illustrated in Fig. 12.

Shear zone and particle rotation

During the shear process, the rearrangement of the shear band can be estimated by reading the average particle rotation [48,49]. As long as the DSST can be used to evaluate the shear band, studying the particle SI effect on the shear band line and the average angular velocity in the model has been considered in this paper. Fig. 13 illustrates the effect of the SI on the particle rotation in the case of a 15% strain under 30 kPa normal stress, the rotation of the particle can be visualized by using a color code illustrating the particles rotation intensity, where the higher rotational particles are shown in a red, medium in green and low rotation particles in blue. Fig. 13 demonstrates that a higher particle rotation occurs for a large and small particle, and the total average rotation for the large particle's SI=150% is lower than the small particle's SI=50%. Figures 13 & 14 illustrate that inter–locking particles increase, and the particle average rota–tion decreases when the SI increases. For instance, as the shape of the particle increases from SI=50% to SI=150%, the total average particle rotation decrease by 66%. Fig. 14 illustrates the average angular velocity for all SI particles. In conclusion, a positive correlation between the shear strength and SI and a negative correlation between the SI and particle rotation [32].

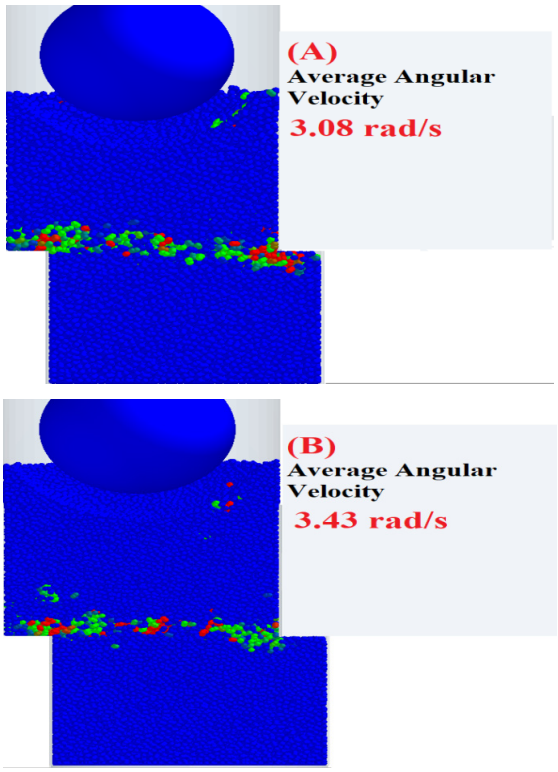

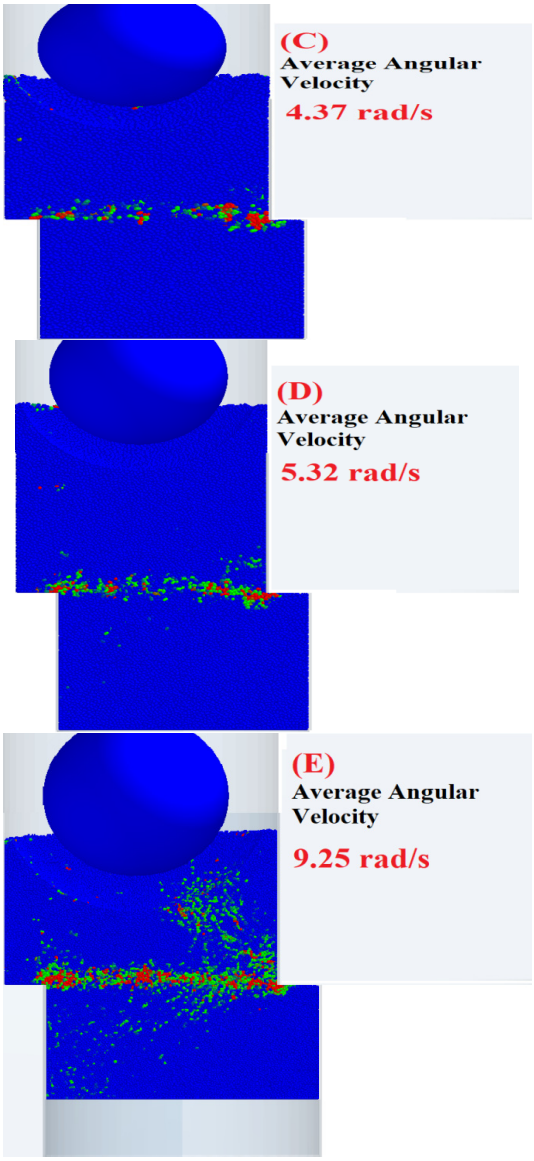

Figure 13 Rotation of particles at 15% shear strain for (SI= 150%, 125%, 100%, 75%, 50% respectively) at 30kPa normal stress

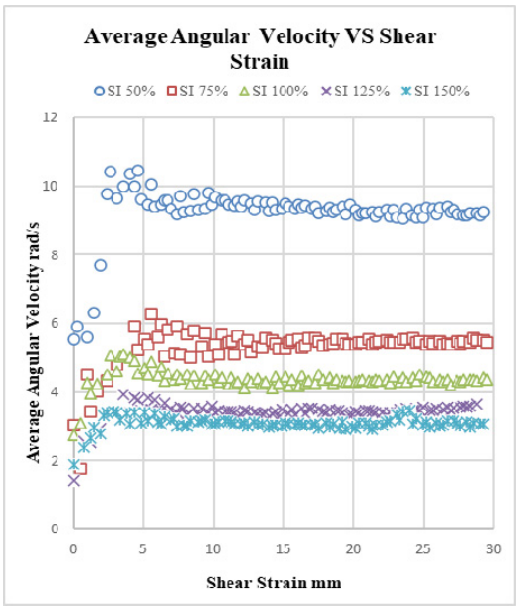

Figure 14 Average angular velocity for different size index particles under 30kPa normal stress

Fig. 15 illustrates the particle's motion behavior, which is described as a movement of horizontal parallel layers, and two factors influence this movement; The normal force begins with, which influences the inter–locking between the particles by increasing the friction between them due to better locking. Therefore the rotation interaction will be increased. In addition, the particle shape where the particle shapes impact the fric–tion intensity among the particles. It can be observed that the particles' rotational patterns follow the direction of the shear band, where the particles with high intense rotation tend to rotate along with the shear band direction.

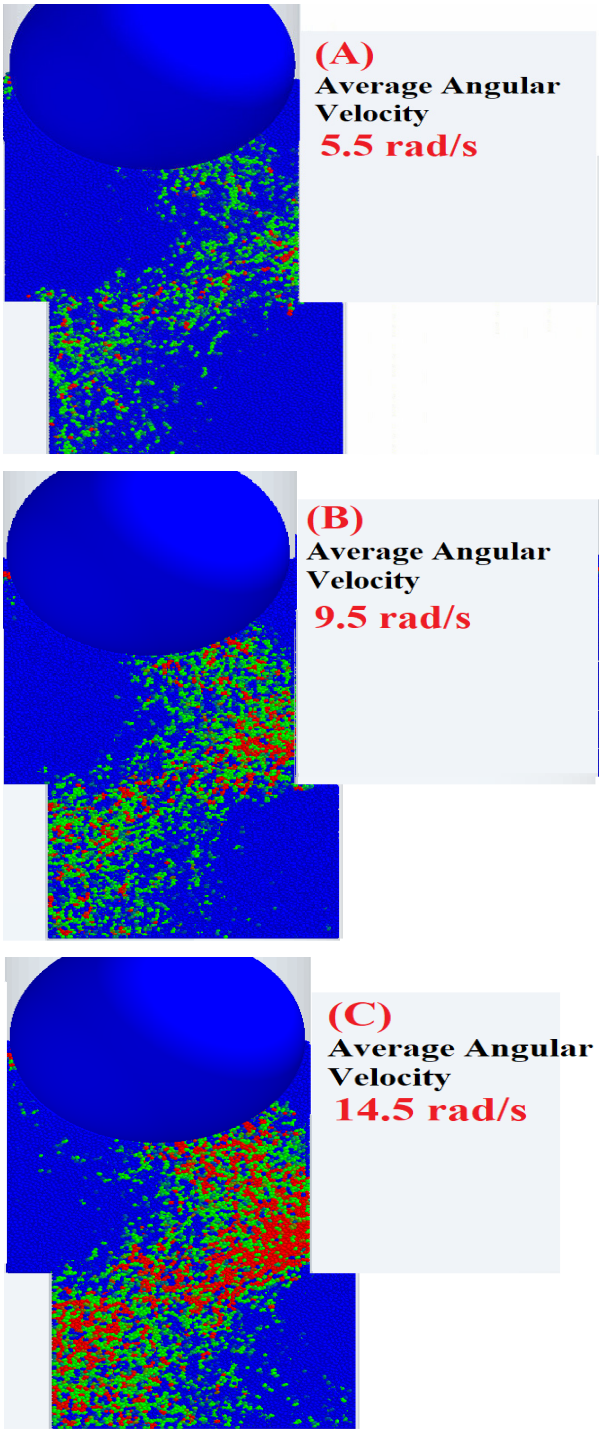

Figure 15 Particle rotation at a shear strain of 15% for a test of SI 75% at different normal stress= 30 kPa, 45 kPa, and 60 kPa, respectively

5. CONCLUSION

This numerical study investigates the effect of particle size on the flow of the bulk granular material. Five particles with different were considered and tested under different normal loads, where the index ranged between 50% to 150% of the particle's actual size. EDEM(3D DEM program)is used to create the particles' shape for a DSST.

The following are the key findings from the exami–nation of both macro-and micro-mechanical properties:

1. Regardless of particle shape, dilation decreases with increasing normal stress in all samples.
2. A positive correlation has been observed between the SI and the particles dilation; however, once the model is subject to a high normal load, the influ–ence of the SI on the dilation becomes insignificant.
3. A positive correlation between the SI and the shear strength has been observed, where the lowest shear strength occurs at the lowest SI value.
4. It does not affect the CN value, and the CN is con–sistent with the dilation behavior of the assemblies. A reduction in the CN accompanies increased dila–tion.
5. The size index SI does not affect the CN value because the SI is not influencing the particles' num–ber of contact within the assembly.
6. As the normal stress increases, the CN Increasing due to better particle interlocking.
7. The movement of horizontal parallel layers desc–ribes the motion behavior of the particles.
8. At the beginning of the shearing stage, the inter-particle forces are uniformly distributed in all assemblies, then the particles CNis relocated with the shear band direction.
9. The average particle rotation is higher for small-sized particles than for large-sized particles due to less particle dilation.
10. The difference significantly influences the particle's micro and macro mechanical behavior of the DSST.

ACKNOWLEDGEMENT

This work was supported by the StipendiumHungaricum Program and the Mechanical Engineering Doctora lSchool, The Hungarian University of Agriculture and Life Sciences, Gödöllő, Hungary.

REFERENCES

[1] Tomantschger K., Petrović V.D., Cerović B.V., Dimitrijević Ž.A, Radojević L.R.: Prediction of a Fertilizer Particle Motion Along a Vane of a Centrifugal Spreader Disc Assuming its Pure Rolling, FME Transactions, Vol. 46, No, 4, pp. 544-551, 2018, doi:10.5937/fmet1804544K

[2] A. M. Remennikov, S. Kaewunruen, “A review of loading conditions for railway track structures due to train and track vertical interaction,” *Structural Control and Health Monitoring*, vol. 15, no. 2. pp. 207–234, Mar. 2008, DOI: 10.1002 /stc.227.

[3] Y. Qian, D. Mishra, E. Tutumluer, and H. A. Kazmee, “Characterization of geogrid reinforced ballast behavior at different levels of degradation through triaxial shear strength test and discrete element modeling,” *Geotech. Geomembranes*, vol. 43, no. 5, pp. 393–402, Oct. 2015, doi: 10.1016 /j.geotexmem.2015.04.012.

[4] B. Indraratna, Y. Sun, and S. Nimbalkar, “Labo–ratory Assessment of the Role of Particle Size Distribution on the Deformation and Degradation of Ballast under Cyclic Loading,” *J. Geotech. Geoenvironmental Eng.*, vol. 142, no. 7, p. 04016016, Jul. 2016, DOI: 10.1061/(ASCE)GT. 1943-5606.0001463.

[5] G. P. Raymond and J. R. Davies, “TRIAXIAL TESTS ON DOLOMITE RAILROAD BALLAST,” *ASCE J Geotech Eng Div*, vol. 104, no. 6, pp. 737–751, 1978, DOI: 10.1016/0148-9062(78)91498-5.

[6] J. Lackenby, B. Indraratna, G. McDowell, and D. Christie, “Effect of confining pressure on ballast degradation and deformation under cyclic triaxial loading,” *Géotechnique*, vol. 57, no. 6, pp. 527–536, Aug. 2007, DOI: 10.1680/geot.2007.57.6.527.

[7] C. N. Cunningham, T. M. Evans, A. A. Tayebali, “Gradation effects on the mechanical response of crushed stone aggregate,” *Int. J. Pavement Eng.*, vol. 14, no. 3, pp. 231–241, Apr. 2013, DOI: 10.1080/10298436.2012.690518.

[8] E. Tutumluer and Y. M. A. Hashash, “Aggregate Shape Effects on Ballast Tamping and Railroad Track Lateral Stability.,” Sep. 2006. Accessed: Jul. 22, 2020. [Online]. Available: https://www.resear chgate.net/publication/237116793.

[9] M. Koohmishi and M. Palassi, “Evaluation of the Strength of Railway Ballast Using Point Load Test for Various Size Fractions and Particle Shapes,” *Rock Mech. Rock Eng.*, vol. 49, no. 7, pp. 2655–2664, Jul. 2016, DOI: 10.1007/s00603-016-0914-3.

[10] D. Li, J. Hyslip, T. Sussmann, and S. Chrismer, *Railway geotechnics*. 2015.

[11] Y. Guo, V. Markine, J. Song, and G. Jin, "Ballast degradation: Effect of particle size and shape using Los Angeles Abrasion test and image analysis," *Constr. Build. Mater.*, vol. 169, pp. 414–424, Apr. 2018, DOI: 10.1016/j.conbuildmat.2018.02.170.

[12] S. Lobo-Guerrero, L. E. Vallejo, "Discrete element method analysis of Railtrack ballast degradation during cyclic loading," *Granul. Matter*, vol. 8, no. 3–4, pp. 195–204, 2006, DOI: 10.1007/s10035-006-0006-2.

[13] S. Abedi, A. A. Mirghasemi, “Particle shape consideration in numerical simulation of assemblies of irregularly shaped particles,” *Particuology*, vol. 9, no. 4, pp. 387–397, Aug. 2011, DOI: 10.1016 /j.partic.2010.11.005.

[14] P. A. Cundall, O. D. L. Strack, “A discrete nume–rical model for granular assemblies,” *Géotechnique*, vol. 29, no. 1, pp. 47–65, Mar. 1979, doi: 10.1680/geot.1979.29.1.47.

[15] L. Rothenburg and R. J. Bathurst, “Micromechanical features of granular assemblies

with planar elliptical particles," *Geotechnique*, vol. 42, no. 1, pp. 79–95, Mar. 1992, DOI: 10.1680/geot.1992.42.1.79.

[16] J. F. Favier, M. H. Abbaspour-Fard, and M. Kremmer, "Modeling Nonspherical Particles Using Multisphere Discrete Elements," *J. Eng. Mech.*, vol. 127, no. 10, pp. 971–977, Oct. 2001, DOI: 10.1061/(ASCE)0733-9399(2001)127:10(971).

[17] Kesler F., Prener M.: DEM: Simulation of conve–yor transfer chutes, FME Transactions, vol. 37, No. 4, pp. 185-192, 2009

[18] E. Tutumluer, Y. Qian, Y. M. A. Hashash, J. Ghaboussi, D. D. Davis, "Discrete element model–ling of ballasted track deformation behaviour," *Int. J. Rail Transp.*, vol. 1, no. 1–2, pp. 57–73, Feb. 2013, DOI: 10.1080/23248378.2013.788361.

[19] X. Bian, H. Huang, E. Tutumluer, and Y. Gao, "'Critical particle size' and ballast gradation studied by Discrete Element Modeling," *Transp. Geotech.*, vol. 6, pp. 38–44, Mar. 2016, DOI: 10.1016 /j.trgeo.2016.01.002.

[20] G. Saussine *et al.*, "Modelling ballast behaviour under dynamic loading. Part 1: A 2D polygonal discrete element method approach," *Comput. Methods Appl. Mech. Eng.*, vol. 195, pp. 2841–2859, 2006, DOI: 10.1016/j.cma.2005.07.006ï.

[21] S. Ji, S. Sun, Y. Yan, "Discrete element modeling of dynamic behaviors of railway ballast under cyclic loading with dilated polyhedra," *Int. J. Numer. Anal. Methods Geomech.*, vol. 41, no. 2, pp. 180–197, Feb. 2017, DOI: 10.1002/nag.2549.

[22] B. Indraratna, P. K. Thakur, and J. S. Vinod, "Experimental and Numerical Study of Railway Ballast Behavior under Cyclic Loading," *Int. J. Geomech.*, vol. 10, no. 4, pp. 136–144, Aug. 2010, DOI: 10.1061/(ASCE)GM.1943-5622.0000055.

[23] [23] G. Jing, K. Feng, L. Gao, and J. Wang, "DEM simulation of ballast degradation and breakage under cyclic loading," *Xinan Jiaotong Daxue Xuebao/Journal Southwest Jiaotong Univ.*, vol. 47, no. 2, pp. 187–191, 2012, DOI: 10.3969/j.issn .0258-2724.2012.02.003.

[24] A. V. Potapov and C. S. Campbell, "A fast model for the simulation of non-round particles," *Granul. Matter*, vol. 1, no. 1, pp. 9–14, 1998, DOI: 10.1007/PL00010910.

[25] A. A. Mirghasemi, L. Rothenburg, E. L. Matyas, "Numerical simulations of assemblies of two-dimensional polygon-shaped particles and effects of confining pressure on shear strength," *Soils Found.*, vol. 37, no. 3, pp. 43–52, Sep. 1997, DOI: 10.3208/sandf.37.3_43.

[26] R. P. Jensen, P. J. Bosscher, M. E. Plesha, T. B. Edil, "DEM simulation of granular mediastructure interface: effects of surface roughness and particle shape," *Int. J. Numer. Anal. Methods Geomech.*, vol. 23, no. 6, pp. 531–547, May 1999, DOI: 10.1002/(SICI)1096-9853(199905)23:6<531::AID-NAG980>3.0.CO;2-V.

[27] T. Matsushima and H. Saomoto, "Discrete element modeling for irregularly-shaped sand grains," *Proc. NUMGE2002 Numer. Methods Geotech. Eng.*, no. May, pp. 239–246, 2002, Accessed: Jul. 22, 2020. [Online]. Available: https://pascal-francis.inist.fr/vibad/index.php?action=getRecordDetail&idt=16398173.

[28] C. Chen, G. R. McDowell, and N. H. Thom, "Discrete element modelling of cyclic loads of geogrid-reinforced ballast under confined and unconfined conditions," *Geotech. Geomembranes*, vol. 35, pp. 76–86, Dec. 2012, doi: 10.1016/ j.geotexmem.2012.07.004.

[29] B. Indraratna, N. T. Ngo, C. Rujikiatkamjorn, and J. S. Vinod, "Behavior of fresh and fouled railway ballast subjected to direct shear testing: Discrete element simulation," *Int. J. Geomech.*, vol. 14, no. 1, pp. 34–44, Feb. 2014, DOI: 10.1061/(ASCE) GM.1943-5622.0000264.

[30] N. T. Ngo, B. Indraratna, and C. Rujikiatkamjorn, "DEM simulation of the behaviour of geogrid stabilised ballast fouled with coal," *Comput. Geotech.*, vol. 55, pp. 224–231, Jan. 2014, DOI: 10.1016/j.compgeo.2013.09.008.

[31] [31] H. Xu and S. J. Liao, "Laminar flow and heat transfer in the boundary-layer of non-Newtonian fluids over a stretching flat sheet," *Comput. Math. with Appl.*, vol. 57, no. 9, pp. 1425–1431, 2009, DOI: 10.1016/j.camwa.2009.01.029.

[32] A. Danesh, A. A. Mirghasemi, M. Palassi, "Eva–luation of particle shape on direct shear mechanical behavior of ballast assembly using discrete element method (DEM)," *Transp. Geotech.*, vol. 23, p. 100357, Jun. 2020, DOI: 10.1016/j.trgeo.2020 .100357.

[33] W. C. Krumbein, "Measurement and Geological Significance of Shape and Roundness of Sedi–mentary Particles," *SEPM J. Sediment. Res.*, vol. Vol. 11, no. 2, pp. 64–72, Aug. 1941, DOI: 10.1306/d42690f3-2b26-11d7-8648000102c1865d.

[34] M. S. Talafha and I. Oldal, "Evaluation the effect of particle sphericity on direct shear mechanical behavior of granular materials using discrete element method (DEM)," *Int. J. Eng. Model.*, vol. 34, no. 1, pp. 1–18, Feb. 2021, doi: 10.31534/eng mod.2021.1.ri.01m.

[35] Talafha M.S., Oldal I.: The effect of Triple Particle sizes on the mechanical behaviour of granular materials using Discrete element method (DEM), FME Transactions, Vol. 50, No. 1, pp. 139-148, 2022, DOI: 10.5937/fme2201139T

[36] Garneau S., Keppler I., Korzenszky P.: Mixing enhancement of wheat granules in a hopper bottom lab-scale mixer using discrete element simulations, FME Transactions, Vol. 48, No. 4, pp. 868-873, 2020, DOI: 10.5937/fme2004868G.

[37] Lommen S.W., Schott D.L., Lodewijks G.: Multibody dynamics model of a scissors grab for co-simulation with discrete element method, FME Transactions, Vol. 40, No. 4, pp. 177-180, 2012.

[38] P. A. . Cundall and O. D. L. Strack, “Cun–dall_Strack.Pdf.” pp. 47–65, 1979.

[39] “DEM Solution. EDEM 2.7.0 User Guide. Edinburgh, United... - Google Scholar.” https://scholar.google.com/scholar?q=DEM Solution. EDEM 2.7.0 User Guide. Edinburgh%2C United Kingdom %282015%29 (accessed Nov. 26, 2021).

[40] I. Old, F. Safranyik, "Extension of silo discharge model based on discrete element method," *J. Mech. Sci. Technol.*, vol. 29, no. 9, pp. 3789–3796, Sep. 2015, DOI: 10.1007/s12206-015-0825-3.

[41] I. Keppler, L. Kocsis, I. Oldal, I. Farkas, and A. Csatar, “Grain velocity distribution in a mixed flow dryer,” *Adv. Powder Technol.*, vol. 23, no. 6, pp. 824–832, Nov. 2012, DOI: 10.1016/j.apt.2011.11.003.

[42] C. González-Montellano, A. Ramírez, J. M. Fuentes, F. Ayuga, “Numerical effects derived from en masse filling of agricultural silos in DEM simu–lations,” *Comput. Electron. Agric.*, vol. 81, pp. 113–123, 2012, doi: 10.1016 /j.compag.2011.11 .013.

[43] V. Kostkanová and I. Here, "Measurement of wall friction in direct shear tests on soft soil," *Acta Geotech.*, vol. 7, no. 4, pp. 333–342, Dec. 2012, DOI: 10.1007/s11440-012-0167-6.

[44] I. Keppler, L. Kocsis, I. Oldal, I. Farkas, and A. Csatar, “Grain velocity distribution in a mixed flow dryer,” *Adv. Powder Technol.*, vol. 23, no. 6, pp. 824–832, 2012, DOI: 10.1016/j.apt.2011.11.003.

[45] J. Gong, J. Liu, “Effect of aspect ratio on triaxial compression of multi-sphere ellipsoid assemblies simulated using a discrete element method,” *Particuology*, vol. 32, pp. 49–62, Jun. 2017, DOI: 10.1016/j.partic.2016.07.007.

[46] L. Rothenburg, R. J. Bathurst, “Numerical simula–tion of idealized granular assemblies with plane elliptical particles,” *Comput. Geotech.*, vol. 11, no. 4, pp. 315–329, Jan. 1991, DOI: 10.1016/0266-352X(91)90015-8.

[47] Y. Yang, J. F., et al: “Quantified evaluation of particle shape effects from micro-to-macro scales for non-convex grains,” *Particuology*, vol. 25, pp. 23–35, Apr. 2016, DOI: 10.1016 /j.parti c.2015.01.008.

[48] M. Oda, H. Kazama, “Microstructure of shear bands and its relation to the mechanisms of dila–tancy and failure of dense granular soils,” *Géotechnique*, vol. 48, no. 4, pp. 465–481, Aug. 1998, DOI: 10.1680/geot.1998.48.4.465.

[49] Z. Mahmood and K. Iwashita, “A simulation study of microstructure evolution inside the shear band in biaxial compression test,” *Int. J. Numer. Anal. Methods Geomech.*, vol. 35, no. 6, pp. 652–667, Apr. 2011, DOI: 10.1002/nag.917.

ИСПИТИВАЊЕ УТИЦАЈА ВЕЛИЧИНЕ ЧЕСТИЦА НА МЕХАНИЧКО ПОНАШАЊЕ ГРАНУЛАРНОГ МАТЕРИЈАЛА МЕТОДОМ ДИСКРЕТНИХ ЕЛЕМЕНАТА

М.С. Талафа, И. Олдал, С. Гарнеуи

Гранулирани материјали се користе у различитим индустријама, укључујући фармацеутску и пољоп–ривредну, где својства материјала елемената имају важан утицај на њихово течење. Нумерички кодови засновани на методи дискретних елемената (ДЕМ) су одлучујући за описивање тока зрнастог мате–ријала. ДЕМ би могао да истражује макро и микро-механичко понашање зрнастих материјала на сми–цање. У ту сврху је коришћен комерцијални софтвер ЕДЕМ® заснован на ДЕМ-у.

Гравитациона диспо–зиција за модел геометријског распореда изведена је у овој студији да би се моделовале различите величине честица за директан, једноставан тест смицања (ДССТ). Резултати су показали да се у односу на индекс величине (СИ) јавља позитивна корелација са смичном чврстоћом, дилатацијом, волуметријском деформацијом, негативна корела–ција са просечном угаоном брзином честице и неут–рална корелација са координационим бројем (ЦН).